Proceedings of ASME Turbo Expo 2014
GT2014
June 16-20, 2014, Düsseldorf, Germany

GT2014-26925

AUTOMATED FINITE ELEMENT MODEL MESH UPDATING SCHEME APPLICABLE TO MISTUNING ANALYSIS

Alexander A. Kaszynski
Turbine Engine Division
U.S. Air Force Research Laboratory
Wright-Patterson AFB, OH 45431
Email: alexander.kaszynski.1@us.af.mil

Joseph A. Beck
Jeffrey M. Brown
Turbine Engine Division
U.S. Air Force Research Laboratory
Wright-Patterson AFB, OH 45431

ABSTRACT

Advancement of optical geometric measurement hardware has enabled the construction of accurate 3D tessellated models for a wide range of turbomachinery components. These tessellated models can be reverse-engineered into computer-aided design (CAD) models and input into grid generation software for finite element analyses. However, generating a CAD model from scan data is a time consuming and cumbersome process requiring significant user-involvement for even a single model. While it is possible to generate finite element models (FEMs) directly from tessellated data, current direct-grid methods produce unstructured grids that can introduce fictitious, numerical mistuning in these models, obscuring geometric mistuning. Nonetheless, as-measured scan data captured in a structured grid is essential for accurate geometric mistuning analyses, provided the tessellated scan data can be rapidly and accurately transformed into a FEM. This paper outlines and demonstrates an approach for rapidly generating structured FEMs for a population of integrally bladed rotors (IBRs) without requiring the arduous task of generating a CAD model for each as-measured IBR. This is accomplished by morphing the structured mesh of a nominal model to the tessellated data set collected from an optical scanner. It is shown that the fidelity and structure of these FEMs can be utilized for accurate mistuning analyses.

NOMENCLATURE

CMM coordinate measuring machine
FEA finite element analysis
FEM finite element model
IBR integrally bladed rotor
ICP iterative closest point
ISA iterative spring analogy
MORPH automated mesh morphing algorithm
RBF radial basis function
TSD tessellated scan data
TWE traveling wave excitation

INTRODUCTION

IBR manufacturing deviations within standard manufacturing tolerances of $\pm$ 2 mil (2/1000 in) ($\pm$ 50.8 μm) can cause dramatic rotor-to-rotor resonant response amplification [1]. This magnification may lead to early part retirement due to microcracks caused by fatigue and could cause catastrophic engine damage due to blade failure. Structural mistuning is a stochastic phenomenon that researchers have addressed through probabilistic approaches [2, 3]. While most published mistuning efforts consider variations in airfoil frequency, recent works have shown that these nominal mode shape mistuning assumptions result in forced response prediction errors on deterministic rotors and probabilistically predicted fleets [4,5]. Therefore, the impact of airfoil geometry variations on resulting mode shapes must be examined across all potential resonant ranges. While recent research has developed reduced-order models to improve solution time when accounting for geometric mistuning [6], this method

requires structured and geometrically accurate FEMs for a population of IBRs. Current geometrically mistuned FEMs have relied on the collection of blade cross sectional data using contact measurement systems that, as it will be demonstrated, are far too approximate to create accurate geometrically mistuned models without a significant increase in measurement time. However, with the advent of highly accurate optical scanners it has become possible to rapidly acquire precise geometric data of an entire IBR thus enabling the engineer to rapidly generate geometrically accurate FEMs.

This paper first outlines current methods for creating FEMs for mistuning analysis and discusses their short comings. It then proceeds to discuss existing algorithms to convert or generate FEMs directly from scan data as well as previous research by the author to automate a FEM to CAD approach. The robust automated mesh morphing approach (MORPH) is then presented to address the short comings of existing FEM reverse engineering methods. The paper concludes with the results and discussions of the MORPH algorithm on a mistuned academic rotor.

TOPOLOGICALLY BASED IBR/BLADE REVERSE ENGINEERING

The discretization of a volumetric domain into a FEM is the computational method of choice for predicting the static and harmonic response of turbomachinery. The standard approach for generating FEMs uses topology-based grid meshing. This topology consists of vertices, edges, and areas that represent a manifold 3D model representative of a component and will henceforth be referred to as a CAD model. The generation of CAD models from in-use hardware, known as reverse engineering (RE), is a well researched method that uses digitized surface coordinates obtained from both contact and non-contact measurement methods [7]. In the past, compressor and turbine blades have been reverse engineered by extracting blade section profiles using a coordinate measuring machine (CMM). Researchers have demonstrated that these CMMs can extract blade geometry repeatability with an accuracy as high as 0.4 mil (10 μm) [8]. High order polynomial splines are fitted to these profiles and the blades are constructed using a series of these splines as described by [9]. These new blade volumes are then linked to a pre-meshed cyclically symmetric disk and volumetrically meshed using the volume sweep method [10] to ensure a structured mesh composition.

The advantages of structured meshing are well known in the finite element community. Hexahedral elements perform well in bending dominated analytical problems due to their reduced computational cost, increased stability, and mechanical response advantages [11]. Linear tetrahedral elements that compose an unstructured FEM tend to overestimate mesh stiffness and introduce error into the analytical solution [12, 13]. While higher ordered tetrahedral elements can lead to more accurate results, these come at the cost of memory and model solution times due to the introduction of mid-side nodes. Specific to mistuning analysis, tetrahedral meshes between blades also introduce numerical discretization variations due to minute changes in internal mesh topology that mask the true geometrically induced mistuning response. Analyzing a population of IBRs can be computationally intractable given the large number of degrees of freedom (DOF) for each model. Therefore, the best practice for modeling blades for mistuning analysis (or FEA in general) is to create hexahedral dominated models to limit computational time and increase the accuracy of the analytical solution.

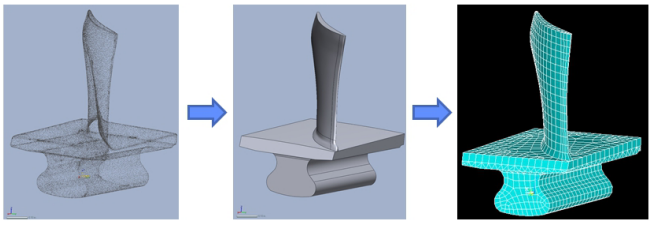

FIGURE 1. TSD to CAD to FEM Workflow

Due to the limitations of current structured meshing algorithms and CMM geometry collection, the classic CAD to FEM RE method is generally confined to a limited portion of the blade and assumes a nominal disk, blade root, and blade tip geometry. CAD models generated from CMM data are reliant on the "as designed" geometry of these areas and can lead to the incorrect computation of blade harmonic response due to the failure to capture potential geometric inconsistencies between the as designed and as built model [14]. In an effort to improve the geometric accuracy of the reverse engineered CAD models from bladed turbomachinery, the author has conducted research into generating CAD models representative of an entire IBR using tessellated scan data (TSD) obtained from an optical 3D scanner [14].

Improved Models Using Optical Scan Data

Modern optical 3D scanners rapidly acquire high density geometric data from physical hardware. The ATOS^{TM} scanner used to collect data for this research relies on the triangulation of projected fringe patterns using two cameras to generate point clouds representative of surface geometry. Each measurement scan from the optical scanner collects 8 million data points that are then post-processed to reduce noise and duplicate results. This reduced point cloud is then converted into TSD through the use of Delaunay triangulation, alpha shapes, or ball pivoting [15]. Though methods for part inspection and quality control from 3D scan data have been widely developed, generating structured computational models directly from tessellated models has undergone limited research despite its potential usefulness in mistuning analysis and FEA in general.

It is possible to extract geometry from the TSD generated

from an optical scanner using a parametric modeling approach. Parametric modeling is a CAD modeling process based on a feature set (i.e. planes, extruded sketches, lofted surfaces, etc.). Figure 1 shows the work flow during which a FEM model is generated from TSD (shown here as a point cloud). The dovetail and platform were modeled as extruded sketches using an extracted profile from the TSD while the blade was generated using the same profile extraction section as the CMM approach, except that the profiles were generated by fitting splines to plane triangle intersection points for multiple sections. The main improvement over a CMM data based approach is the ability to capture the entire geometry of the model and have direct feedback during the modeling process on the accuracy of the RE part. While parametric modeling has proven to be a viable approach for generating accurate and structured mesh compatible CAD models [16], geometric approximations were still made during the CAD process. The thickness of the blade root was underestimated by as much as 10 mil ($\pm$ 254 μm), since a constant radius fillet was not computable within the CAD software due to the adjacency of the root to the platform corner. Additionally, minor variations in the blade surface geometry between the captured profiles were not translated into the NURBS surface based CAD model due to the construction of blade profiles.

Additionally, the effort required to generate this CAD model was considerable. The volume had to be edited within both CAD software and grid generation software to make it applicable for a hexahedral-dominant meshing scheme. For this relatively simple blade, the entire TSD to CAD process took approximately 4 hours and creating the hex gridable geometry took an additional 2 hours. Scripting the process to automatically generate the bladed portion of the model was the main contribution of the author's previous work. This script, while functional in an academic environment, was not sufficiently robust to be applied to non-academic rotors and would require heavy user intervention during model creation and meshing. Defects in the TSD would lead to solid modeling failures and the meshing script would have to be modified to account for variations between rotor models to avoid grid generation failures. This demonstrates that the main difficulty in the RE FEM process, both using CMM and optical geometry, is robustly generating a CAD model of sufficient fidelity to match the in-use hardware while remaining compatible to structured meshing.

Removing CAD from the work flow and relying directly on the TSD would both accelerate the grid generation process and increase its robustness when analyzing a population of highly-variant parts. Given the high point density and accuracy of the current generation of optical scanners, a fast and efficient approach for generating a computational model would be to obtain a grid mesh directly from the TSD. The next section will assess existing methods that generate FEMs from scan data, identify their shortcomings, and propose a new approach to generate FEMs from optical scan data.

DIRECT TSD TO FEM GENERATION

The most direct approach for creating a FEM directly from TSD would be to replace surface point cloud data with FEM nodes and use Delaunay triangulation to generate internal elements. However, the aspect ratios of the triangles composing the TSD are generally unsuitable for finite element analysis since triangle aspect ratio is not considered during TSD assembly. Additionally, the density of the FEM elements would be dependent on the density of the original point cloud which gives the engineer no control over mesh density and makes it impossible to conduct a mesh convergence study. One solution to the shape and density problem of the triangles composing the TSD is to recompute the surface mesh using geodesic remeshing [17] by replacing the initial surface mesh with one containing well shaped triangles and a density chosen by the user. While this would allow for the creation of a FEM with well shaped elements from TSD, the model would still be limited to tetrahedral elements. While this approach could be improved with higher order elements which have increased accuracy and improved response prediction, an unstructured grid fails to meet the model requirements for mistuning analysis due to the aforementioned reasons.

To date, there exists no method to automatically generate a structured mesh directly from a tessellated surface. While there are several methods which can automatically generate hexahedral meshes from complex CAD by dividing up volumes into mesh sweep compatible sub-volumes [18], these methods are incompatible with TSD assembled from point clouds since they are still dependent on topological based models. Even if methods could be made to work around topological mesh dependence, TSD are often marred with missing data due to line of sight issues which obscure the geometry of the internal IBR bore or other disk surfaces. A pure TSD to FEM method would require a manifold TSD as the tessellated surface must be continuous to generate a volumetric mesh. While it is possible to have meshing software automatically repair small and straightforward discontinuities in a tessellated surface mesh [19], larger mesh discontinuities from scanning limitations or line of sight issues would require user intervention to create a zero boundary TSD.

An optical scanner cannot be relied upon to consistently produce a manifold tessellated surface and there is no working approach to generate a structured mesh directly from the TSD. A solution would be to generate a high fidelity, well shaped, structured FEM from TSD using the "best of both worlds" approach of combining the mesh control of a topologically based mesh with the high fidelity, geometrically accurate approach of a pure TSD to FEM method. Commonly used in the graphics community, mesh metamorphosis uses harmonic mapping to smoothly transform the mesh of one 2D or 3D object to a new object [20, 21]. Applied to FEA, this would solve the problem of inconsistent element quality associated with meshing directly from optical scan data and would allow for an automatic mesh formulation method by relying on a single nominal FEM and modifying it to match

optical scan data from in-use hardware.

Hardisty and Whyne used this approach to generate FEMs of various rat vertebrae [22]. A single FEM of a rat vertebrae was created from CAD and the surface was harmonically mapped to a unit sphere. This parametric map served as the source mesh and the basis of all future models. Further scans were parametrically mapped to unit spheres and these target meshes were mapped to the source mesh using triangular barycentric coordinates for each triangle/vertex intersection. However, this approach proved to be far too inaccurate to generate a sufficiently aligned mesh for mistuning analysis as the average deviation between the new FEM and the vertebra geometric data was determined to be 7.4 mil (188 μm). Considering the standard manufacturing deviations for IBRs are $\pm$ 2 mil ($\pm$ 50.8 μm) and the optimal FEM accuracy should be at least an order of magnitude smaller to capture geometric mistuning, this harmonic mapping approach has insufficient fidelity to be applied to mistuning analysis. Additionally, harmonic mapping provides no direct correspondence between the elements on the source and those on the target. Elements located on the high density portion of the source FEM may not end up on same relative location on the target FEM.

Due to the limitations of current mesh morphing approaches as well as the lack of direct TSD to FEM generation algorithms, a new mesh metamorphosis approach has been developed.

An Intelligent Mesh Morphing Method (MORPH)

The proposed mesh morphing strategy allows the user to finely control the density and quality of the mesh for a population of parts without having to regenerate CAD models and the associated volumetric grids for an entire population of rotors. When applied, this methodology, MORPH, will increase the accuracy of the mistuning analysis while simultaneously decreasing the time spent on model generation, often the most time consuming step of the analytical process.

The first step is to generate a "seed" FEM that serves as an initial model which, through MORPH, becomes representative of the scanned part. Optical scan data is parametrically RE and then imported into grid generation software to produce a hex-dominated FEM using the aforementioned parametric RE process. Depending on the part-to-part variation, this RE CAD can either be generated from a single TSD from the scan population or from an averaged TSD from a population of separate part scans. A comparison between these seed model generation approaches will be discussed in the results section to determine the hysteresis of MORPH. While the parametric RE method is still an approximation of the actual part geometry, limitations in CAD and grid generation will be corrected through MORPH.

After creating a seed FEM, the next step is to align the population of scan data with the seed model by translating and rotating each TSD to match the location and orientation of the seed FEM. One challenge with optical scanning is the lack of a common

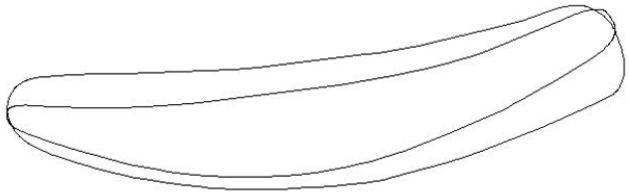

FIGURE 2. IBR Blade Root Cross Section Variation

reference frame between point clouds. Optical scanning systems generally use the scanner head as the reference frame whose location and orientation can vary across multiple part scans. The solution to the reference frame problem is to align the scan data to the FEM using the well established Iterative Closest Point (ICP) method [23]. The external nodes of the FEM are treated as the source point cloud and the vertices of the TSD as the target point cloud. A rigid body transformation is then computed to minimize the distance between the source and target by rotating and translating the target point cloud to the source. ICP can be optimized for turbomachinery by providing weights to certain portions of the structures (e.g. dove tail contact areas) to emphasize the alignment of those areas. Having aligned the scan data to the FEM, the external and internal nodes of the FEM are now ready to be updated to match the geometry of each scanned part.

Initial testing of the mesh morphing method on fielded turbomachinery hardware revealed an increased potential for significant part-to-part variation which could potentially corrupt a morphed mesh unless steps were taken to conserve element orthogonality and aspect ratio. For example, it was discovered that there was a bimodal distribution of root section thicknesses for a population of IBRs due to a change in manufacturers over the course of the production of the rotor as shown in Fig. 2. Additionally, in the case of the academic IBR, later analyzed in this paper, large deviations in leading and trailing edge thicknesses as well as relative section locations necessitated the creation of a highly robust and intelligent morphing algorithm.

For very small relative deviations, modifying the node locations by moving them directly along their respective normal vectors would be sufficient to update the model to match the scan geometry. However, several problems arise from all but the smallest of node displacements. Elements can become inverted or skewed if external nodes are displaced while internal nodes are kept fixed within the FEM. Furthermore, the new FEM could also have corrupted elements if the node displacements create overlapping "bow-tie" faces across the exterior of the model. Figure 3 illustrates this potential node normal intersection problem that commonly occurs for blade tips when the actual scan data is within the nominal FEM. The FEM, denoted by outside lines representing element edges and dots representing nodes, is projected onto the thin inside line representing the TSD using node normal vectors. Due to the convex nature of blade edges, the

node normals will overlap or fail to intersect the TSD if the scan data or FEM are significantly misaligned. The FEM node normals cannot be modified so that these intersections would not occur as this would eliminate correspondence between the nominal and MORPHed FEM. For example, the normal vectors at the blade tip in Fig. 3 would not be projected onto blade tip of the TSD even with a large change in their normals, and if this were attempted, it would severely corrupt the new FEM and result in an inaccurate computational analysis.

In order to overcome these and other challenges, a new adaptive, iterative mesh morphing algorithm was developed. MORPH is an iterative multi-step approach that intelligently modifies FEM node positions based on the geometry of both the FEM and TSD while maintaining element shape and mapping.

Algorithm

1. Compute FEM surface node normal vectors.
2. Calculate node displacement vectors using a score based alignment method using FEM to TSD distance and alignment.
3. Distribute local node displacements among adjacent nodes using a radial basis function (RBF).
4. Sum the RBF displacement vectors for all nodes and update node positions. Limit maximum node movement by a fraction of the global average element edge length.
5. Check updated element shape. Limit node movements that would corrupt surface elements (e.g. aspect ratio and skew).
6. Iterate through steps 1-4 and modify the RBF based on the rate of change of node positions. Run until FEM to TSD distance converges.
7. Place surface mid-side nodes of quadratic elements between edge nodes. Compute mid-side node normal vectors based on the average of the edge node vectors and move those nodes directly along the normal vectors to the TSD.
8. Update the positions of internal nodes using the iterative spring analogy (ISA).

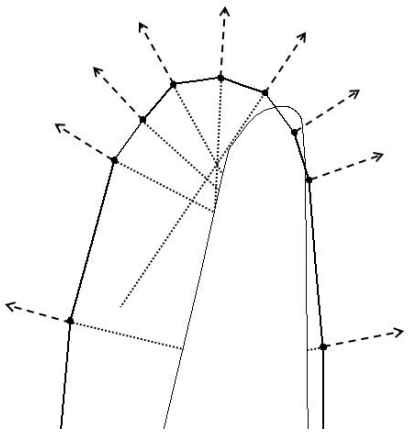

FIGURE 3. Potential Node Normal Intersections at Blade Leading Edge

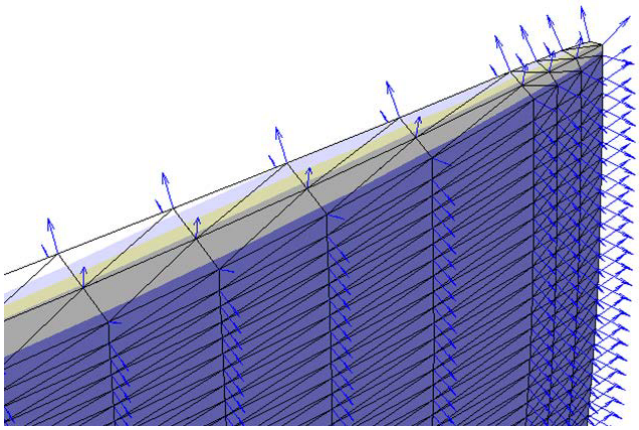

FIGURE 4. Node Normal Vectors on a Blade Tip

At the start of each MORPH iteration, normal vectors were computed for all surface nodes of the FEM. These normal vectors were calculated using an edge length weighted average of the cross products of all element edge pairs adjacent to each node. Figure 4 shows an example of node normals computed from a FEM of a 3D blade tip. An initial FEM to TSD estimate was computed using the intersection of these node normal vectors and the surface of the TSD. Using the node normal to TSD intersection distance rather than the nearest point cloud vertex vastly improves the accuracy of the initial FEM to TSD estimate by taking into account the shape of the FEM surface while ignoring the potential variation in point cloud density that would affect the distance results. However, with as many as 10^6 FEM surface nodes and 10^8 TSD triangles, a brute force computation could require 10^{14} calculations to compute node normal to TSD intersections for IBR models.

To accelerate and vectorize this computation, the Fast, Minimum Storage Ray/Triangle intersection algorithm from Möller et al. [24] was applied to reduce memory requirements for large scan data files. Each FEM node normal N is defined by origin O, location of the node, and direction D representing the normal vector of that node as shown below.

$$N(t) = O + tD \tag{1}$$

The n x 3 matrices O and D were assembled for the entire FEM to facilitate vectorization within MATLAB. To compute the intersection locations for each triangle, the coordinates of each triangle composing the TSD was converted into a natural coordi-

nate system. The equation for a point on a triangle in barycentric coordinates (u,v) follows where V_0, V_1, and V_2 represent the vertices of the triangle.

$$T(u,v) = (1-u-v)V_0 + uV_1 + uV_2 \tag{2}$$

Setting $N(t) = T(u,v)$ allows for the computation of the TSD and node normal intersection. The solution required an n x 3 origin matrix, n x 3 vector matrix, and a t x 3 x 3 triangle vertex matrix where n is the number of nodes and t is the number of triangles. Each intersection is computed by solving a set of linear equations from Eqn. (2) for each triangle. The memory requirements for the intersection computation were reduced by limiting the t x 3 x 3 triangle vertex matrix to only the nearest t_s triangles for each node. These triangles were selected using MATLABs built-in nearest neighbor algorithm *knnsearch* based on Euclidean distance.

This FEM to TSD distance is used as an initial estimate of a FEM node's alignment and proximity to the TSD. A node is considered aligned to the TSD if its distance is 0.1 mil (5.08 μm) to the TSD. The local displacement vector of these aligned nodes is directly along their node normal vectors towards TSD. The local displacement vectors of all other nodes that exceed this minimum displacement distance are estimated using the best scoring tessellated face near each individual node. Every misaligned node is assigned a limited set of proximate faces to encompass potential FEM to TSD alignments and limit computation time. Each one of these faces is then scored based on its distance between the node and its relative alignment to that node's normal vector. This score S is computed by the equation

$$S = \frac{d_{min}\frac{1}{d_f} + \hat{n}_f \otimes \hat{n}_n}{2} \tag{3}$$

where d_f is a vector of the distances between the FEM node and the center of adjacent TSD faces. This distance is normalized by the minimum distance d_{min} between the FEM node and a tessellated face so that one face will always score unity. The right hand side of the numerator describes the normal vector alignment score where $\hat{n}_f$ is an array of normal vectors of the surrounding faces and $\hat{n}_n$ is the normal vector of the node of interest. The face with the highest score is considered the face with the highest likelihood to have a similar topology to the current node. Provided the score is above a minimum threshold, the node is projected upon the plane of the face and moved in the direction of the normal vector of that face. This approach of moving surface nodes provided the highest rate of convergence and ensured element mapping between topologically similar surfaces on the FEM and TSD.

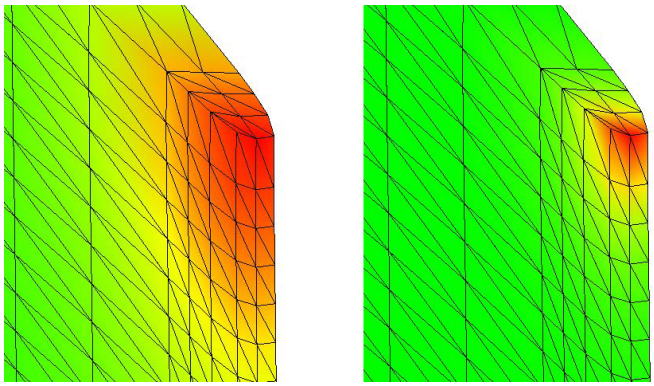

FIGURE 5. Large and Small Node Influence Using a Gaussian RBF

Having obtained local node displacement vectors, the next step is to distribute these displacements to neighboring nodes using a RBF. This helps to minimize the possibility of surface element crushing and allows for the alignment to misaligned TSD. Nodes originally not on the surface of the TSD and unpaired with a sufficiently high scoring face on the scan data will be moved closer into alignment without corrupting nearby surface elements due to the displacement vectors of their aligned neighbors. For example, if the blade tip shown in Figure 4 was actually longer than estimated in the nominal model, the nodes with normal vectors pointing directly upward would move to the surface of the TSD, but without distributing local node displacements, only the nodes in the center of the blade would move to capture the actual blade length. The nodes of the edge, but not center, of the blade would remain stationary since their normal vectors are 45° to the blade tip and would intersect with the pressure or suction surfaces rather than the blade tip. By allowing nodes to influence their neighbors through the Gaussian RBF φ, poorly aligned nodes can move closer to the TSD despite that their movement paths may not be in the same direction as their node normal vectors. The node-to-node influence is dependent on the geodesic distance between two nodes through the 3D FEM and is given by

$$\varphi(r) = \tau e^{-(\varepsilon r)^2} \tag{4}$$

where τ is the linear influence coefficient, ε is the exponential influence coefficient, and r is the geodesic distance through the 3D mesh. By varying the parameters τ and ε between iterations, the model can be globally flexible during the initial iteration steps and then allowed to converge at the local level as the FEM to TSD distance begins to converge. Figure 5 shows the large range of node influence at the start of MORPH and a more localized range of influence near the end of the iterative process.

At the end of each iteration and prior to moving the nodes,

each FEM node has its own displacement vector computed by either moving it directly along its normal vector to the TSD or along the planar distance to the highest scoring triangular face on the TSD. This yields a n x 3 displacement matrix D which is then multiplied by the n x n influence matrix from the Gaussian RBF computed from the geodesic distances of each node to its surrounding neighbors.

$$v_i = v_{i-1} + \varphi(r) \otimes D \tag{5}$$

Equation (5) shows how the tensor product between the node influence array φ and the displacement matrix D produces a final displacement vector for each node that takes into account the neighboring node displacement vectors. Summing this product with the current node location array v_{i-1} yields the new node position array. The surface elements, given these new node positions, are then checked if they exceed shape warning limits in aspect ratio or skew. Elements that exceed these limits have their nodes "relaxed" to increase the orthogonality of the surface element. This check and relax method was achieved by splitting all surface FEM elements into triangles and observing the relative change in triangle angles between iterations. Node movements that caused large relative movements were then moved along the surface of the FEM to improve the orthogonality of the structured mesh.

The displacements of each iteration are limited by a fraction of the global average edge length so that the node normal vectors can be updated at the start of the next iteration. This allows for a smooth transition of the FEM node normal vectors so that they come into alignment with the TSD face normal vectors. The iterative MORPH algorithm continues until all the nodes of the FEM lie on the TSD or the FEM to TSD error converges. In the second case, it may indicate there are portions of the FEM that are geometrically divergent. This occurred during algorithm testing when the optical scanner encountered line of sight issues with the component of interest. In the case of the academic IBR, it was not possible to scan the bore in its entirety and the nominal FEM was left unmodified for that portion, demonstrating that MORPH does not require manifold TSD to operate properly.

The next step after aligning the surface nodes of the FEM is to update the positions of the internal nodes. It was found that the most effective approach was to use ISA to control internal node deformation. Commonly used when updating meshes between Computational Fluid Dynamics (CFD) iterations [25], ISA allows the CFD programmer to introduce boundary condition displacements (e.g. at an airfoil surface) and propagate those new boundary node displacements throughout the remainder of the mesh. In the case of a 3D FEM, the ISA is used to update internal nodes so that their positions are modified given the displacements of the external nodes. The ISA uses the simplified governing equation for vibrations given as

$$Ku = F \tag{6}$$

where K is the stiffness matrix and u is the displacement vector of internal and external nodes. Nodal force F is set to zero as neither the boundary nodes nor the internal nodes are moving. The stiffness matrix is assembled using the direct stiffness method with the inverse of the length between nodes representing stiffness for that nodal linkage. The displacement vector is then populated with the known displacements of the surface nodes and the equation is solved for the unknown displacements of the internal nodes. This equilibrium problem can be solved using Cholesky decomposition or the Gauss-Seidel method.

Once the positions of the internal nodes have been computed, the mid-side nodes of higher order elements (if applicable) are placed between their corresponding edge nodes. The positions of these nodes are then moved to the surface of the TSD by computing the intersection distance between the TSD and the normal vector from the mid-side node. Since the surface element edge nodes have been aligned to the surface of the TSD, the movement of the mid-side nodes will capture the non-linear variation in geometry between the aligned edge nodes. Quadratic elements at blade tips vastly improve the accuracy of the analytical solution without requiring a computationally intensive element density to capture the non-linear geometry using linear hexahedral elements.

MORPHING THE PURDUE TRANSONIC ROTOR

The developed methodology was applied to an academic IBR shown in Fig. 6. The Purdue Transonic Rotor is a highly mistuned 18 blade IBR with blade to blade deviations as high as 10 mil (254 μm), roughly 5% of the blade thickness. These deviations, as previously mentioned, can lead to stress amplifications within IBRs due to mode coupling and must be captured within FEA for accurate mistuning analysis.

The scan data for three rotors was collected using the commercially available blue light scanner ATOS III. The seed mesh was generated by first creating an average IBR sector from three measured rotors by using ICP to register the TSD from all three rotors to a common coordinate frame centered at the bore of the disk. The aligned scan data from each rotor was then merged to create an averaged IBR which was then averaged cyclically to create a nominal section TSD. The nominal disk and blade sector was RE using a traditional CAD approach of parametrically modeling the disk and lofting the blade section using the commercially available software Rapidform^{TM}. This model was then imported into ANSYS and meshed using a predominately hexahedral mesh with a tetrahedral and pyramidal interface between

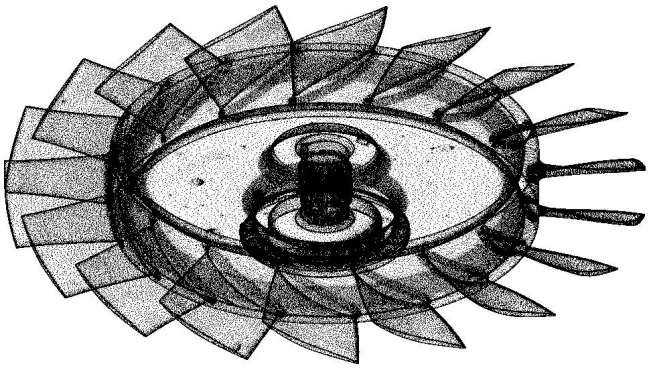

FIGURE 6. Purdue Transonic Rotor Point Cloud

the hexahedral blade section mesh and hexahedral disk section mesh. This section was replicated about the center of the disk to generate a full cyclically symmetric FEM consisting of 113,058 elements and 137,016 nodes with each blade containing 3,234 hexahedral elements and 5,138 nodes.

The accuracy of the nominal FEM was checked against a member of the academic transonic rotor population to compare the deviation between the nominal FEM and the scan data obtained from an IBR. Figure 7 shows the blade alone deviation for both the front and back of the IBR. This deviation was calculated by computing the normal distance between the FEM and the TSD using the previously described node normal method. The green contours show deviations of the model within $\pm$ 2 mil ($\pm$ 50.8 μm) of the nominal model. Red contours indicate the TSD lies outside the FEM while blue contours indicate it lies within. This mistuning pattern apparent in the deviation analysis was not intentional and was likely caused by tool wear given the periodic variation of blade thickness.

The FEM was exported from ANSYS and imported into MATLAB to begin the iterative MORPH procedure. As mistuning analysis is primarily concerned with the geometric deviations between blades where stress amplifications are most likely to occur, only the blade portions of the FEM were exchanged. However, it should be noted that the robustness of the MORPH code enables the user to MORPH the entire IBR if desired. Recall from the methodology section that the iterative process starts with computing the normal vectors from the FEM and estimating an initial displacement based on the intersection distance along the normal vector to the scan data. Based on that distance, nodes were either considered aligned or misaligned and had their positions updated either by moving them directly along their node normal vectors towards the TSD or given a best guess displacement vector dependent on TSD to FEM alignment and distance. These distances were then distributed using a Gaussian RBF and the mesh was then deformed based on the sum of all RBF node displacement values. The number of mesh updating iterations required for convergence varied between 20 and 50 depending

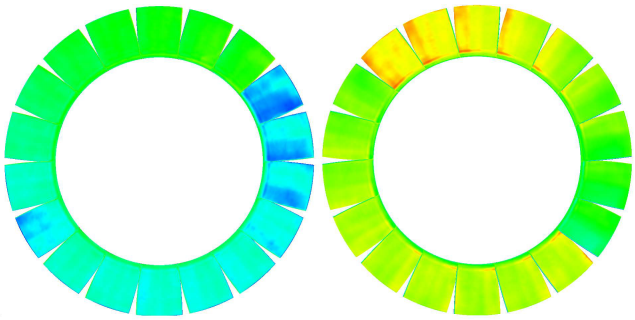

FIGURE 7. Purdue Transonic Blade TSD to Nominal FEM Deviation

on how misaligned the individual blade was from the nominal model. It took approximately three seconds for an iteration of each blade with a total solution time of 15 minutes for all blades of the IBR. The computer used for mesh updating had 16 cores running at 3.1 GHz and 64 GB of memory utilizing a 64-bit operating system.

MORPH Results

The nominal and MORPHed FEM can be seen in Figures 8 and 9 respectively. The largest apparent change between the nominal and MORPHed model is the curvature of the blade tip and the change in leading and trailing edge thickness. As mentioned in the previous work section, one of the challenges in solid model reverse engineering is the limitation of the meshing software when generating a structured grid on extracted RE surfaces and parametric features from scan data. In the case of the Purdue transonic IBR, the blade tips could not be accurately modeled due to the mesh sweep method used to generate a structured grid on the volume. MORPH was able to capture these grid generation shortcomings as well as geometric variations due to blade manufacturing deviations as apparent in Fig. 7. The MORPH al-

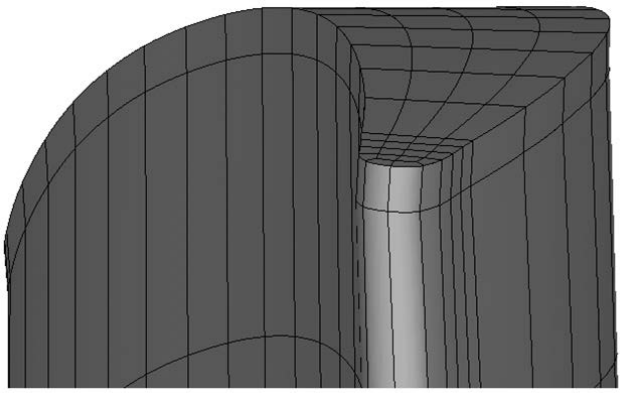

FIGURE 8. Nominal Blade FEM from the Purdue Transonic Rotor

gorithm was able to converge on a geometrically mistuned solution with the average pre and post FEM node to TSD blade error being 5.5 mil (139.7 μm) and 0.07 mil (1.78 μm) respectively.

Three geometrically mistuned FEM models have been produced from this IBR to evaluate and compare the relative effectiveness of MORPH in producing a geometrically mistuned FEM. A FEM built from CMM touch probe data, the SABRE method from [14], and a tuned FEM built from SABRE by averaging multiple blade sections that also served as the seed mesh for the MORPH method. Post processing of the academic IBR FEMs included the computation of the total volume of each blade to provide a basis of comparison between FEM models. This was accomplished by separating each blade from the disk and computing its manifold volume from the FEM. Figure 10 shows the volumetric variations between the all blades compared to the

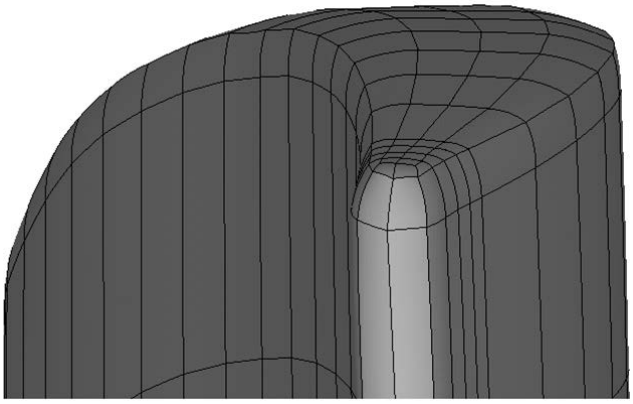

FIGURE 9. MORPHed Blade FEM from the Purdue Transonic Rotor

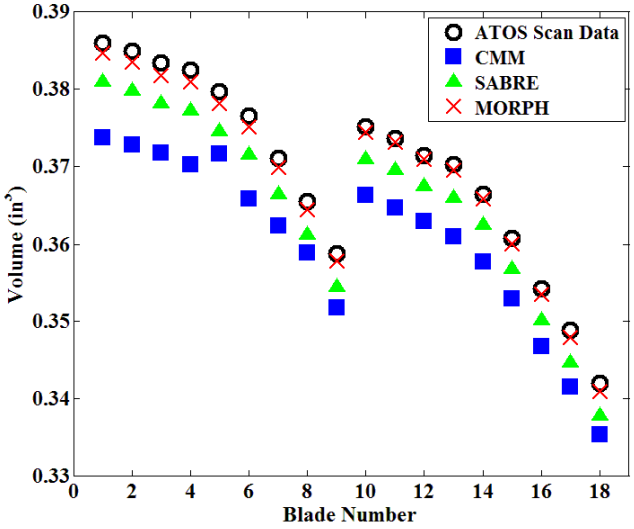

FIGURE 10. RE FEM Blade Volume Comparison

TABLE 1. REPEATED SCANS HARMONIC VARIATION

Mode Shape	σ (Hz)	$\frac{\sigma}{\mu_{ms}}$
1B	0.896	0.070%
1T	1.694	0.056%
2B	3.039	0.062%
2B1T	5.109	0.076%

ATOS optical scanner. The unintentional manufacturing mistuning pattern is apparent in the periodic volume variation. On average, the FEM generated from the CMM had a blade to scan volume error of 9.61 x 10^{-3} in^3, 4.56 x 10^{-3} in^3 for the SABRE model, and 1.02 x 10^{-3} in^3 for the MORPH FEM. Based on these results, it is clear that MORPH produces the most geometrically accurate FEM relative to the TSD given its improvement in volumetric accuracy over models built using traditional methods. The FEM produced with MORPH showed a remarkable agreement with the optical scan results as the volume within 0.28% of the TSD results. Therefore, it is possible to create a geometrically mistuned model nearly identical to the in-use hardware provided the geometry obtained from the optical scanner is accurate.

Given the MORPH's reliance on TSD, it is crucial to ensure that the 3D coordinates collected from the ATOS scanner are representative of the actual geometry of the in-use hardware. Research by [26] indicates that the ATOS II scanner achieves a 0.394 mil (10 μm) accuracy at a 95% confidence level. This agrees with the conclusion from the author's research [14] that indicated the ATOS III scanner was accurate within to 0.3 mil (7.62 μm). Considering that the MORPH algorithm may be more sensitive to noise than models built using CMM or SABRE, five repeated scans were collected from a single IBR to determine the harmonic variation given these repeated scans. To induce more noise, these scans were collected without coating the IBR with an anti-reflective coating that reduces lens glare and increases the accuracy along highly reflective and convex surfaces (i.e. blade tips). Using the same seed model, 5 FEMs were created and a modal analysis was conducted within ANSYS to extract disk/blade harmonics. Table 1 shows the frequency deviation for the first 4 mode shapes of the IBR. While optical scanner noise impacts the results, the harmonic deviation due to this noise is relatively small ($\mu = 0.066\%$). It should be noted that combining and averaging multiple scans improved the accuracy of the harmonic analysis more than averaging the harmonic results since the averaged TSD improved blade tip accuracy.

Variations in the relative shape, alignment, and accuracy of the seed mesh have the potential to drive large changes in the harmonic results from a mistuned model. Two separate seed models

TABLE 2. SEED MESH HARMONIC VARIATION

Mode Shape	T vs. MT	S vs. MS	MT vs. MS
1B	1.393%	0.294%	0.010%
1T	0.997%	0.243%	0.024%
2B	1.018%	0.197%	0.019%
2B1T	1.137%	0.216%	0.020%

were used to evaluate the sensitivity of the MORPH algorithm on the initial seed FEM. The tuned nominal seed mesh was generated using an averaged disk section obtained from CAD software. The initial FEM to TSD error was 5.5 mil (139.7 μm). The second seed mesh was the FEM obtained from the SABRE method which, prior to this work, had the best approximation of geometry of all previous RE FEM methods. The initial blade FEM to TSD error was 1.3 mil (33 μm), and while this demonstrates the coarse geometric approximation that SABRE achieved, the model still shows a vast improvement over using a tuned nominal model for mistuning analysis. Using identical algorithm control parameters, both seed FEMs were MORPHed to the same TSD and then evaluated harmonically within ANSYS. Table 2 shows the results with abbreviated names for each FEM seed and MORPHed model, where T stands for the tuned nominal FEM, MT for the MORPHed FEM using the tuned FEM as a seed mesh, S the FEM from the SABRE method, and MS the MORPHed model using the SABRE FEM as a seed mesh.

Given the large geometric mistuning between blades, the 1.3% harmonic variation between the tuned and mistuned models was expected. The 0.24% variation between the FEM SABRE and the MORPHed SABRE FEM demonstrates the importance of taking into account the mistuned geometry of the entire IBR rather than limiting the FEM mistuning to central blade geometry. Most importantly, the 0.018% harmonic variation between the two MORPHed models demonstrates the robustness of the MORPH algorithm given the near identical harmonic results despite the varied seed meshes. One potential source of error from the MORPH algorithm is from poorly shaped elements arising from high seed FEM to TSD variations. The limited node displacements from the already well shaped SABRE FEM elements had the potential to produce a more accurate FEM than the highly displaced nodes from the average CAD FEM. However, this was not the case despite the extraordinary geometric mistuning present between blades from the Purdue Transonic Rotor. This was most likely due to the iterative node updating approach which ensured that elements were not crushed due to displacements along inaccurate node normal vectors. The MORPH algorithm displays virtually no hysteresis due to a varying seed mesh

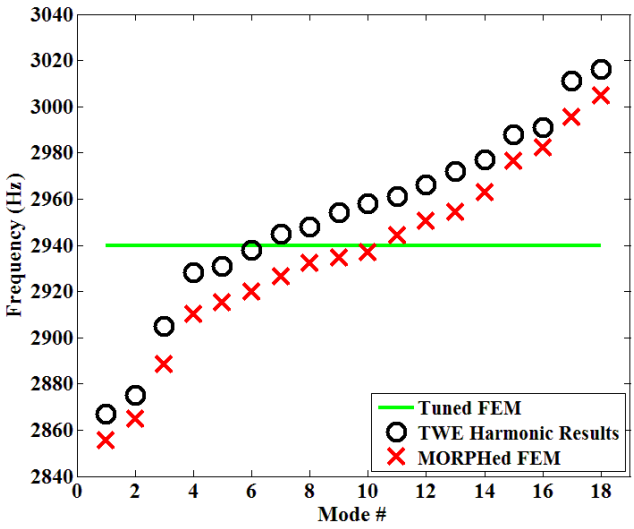

FIGURE 11. Experimental Validation of MORPH for 1st Torsional, Zero Engine Order Harmonic Results

provided it matches the general topology of the target TSD.

To validate the MORPH algorithm as with experimental data, a Traveling Wave Excitation (TWE) Scanner owned and operated by the US Air Force at Wright Patterson Air Force Base was used to extract IBR resonances for the first 10 kHz. The TWE operates by exciting each blade either in phase or out of phase to simulate engine order excitation over a specified frequency range to determine blade forced response and has been used with success to determine IBR harmonic response [27]. Experimental results from the Purdue Transonic IBR using the TWE show a high correlation to the harmonic analysis results from the MORPHed FEM as per Fig 11. The figure shows the 1st torsional tuned and mistuned harmonic responses from FEA as well as the results from the TWE for the same mode shape. These results indicate a high correlation between the damped modes extracted from the TWE and the undamped modes extracted from the 1st torsional mode FEA. As the 0.3% bias between the TWE and mistuned results occurs consistently throughout the first 108 modes and it can likely be assumed that the variation between the assumed and actual material properties are the primary driver in the bias between the experimental and computational results. Additional variation may be due to the fact that the natural frequencies extracted from the TWE were damped while the modal analysis within ANSYS was undamped as the damping value of the IBR was unknown at the time of the analysis. There also remain uncertainties in the experimental results to include the free-free assumption made on the basis of previous research as well as calibration and repeated test dissimilarities which should be addressed in future work. However, these results indicate that the FEM MORPH approach produces harmonically consistent results to experimental data and it has excellent potential for

modeling fielded hardware computationally.

CONCLUSION

This paper developed an IBR/blade RE process sufficiently automated so that a fleet of parts could be measured and analyzed without relying on user-CAD interaction for the creation of individual FEMs. The MORPH mesh updating approach was demonstrated to be robust, accurate, and independent of the relative accuracy of the seed FEM. MORPH allows the FEA engineer to use an as-designed CAD and FEM while still capturing the harmonics of a mistuned IBR.

The repeatability of the RE method described here makes it a viable option for future depot work to verify IBR mistuned response. The FEA results from the mistuned models can be used for forced response prediction as well as fatigue estimation for manufactured IBRs and blades. While this research has verified the accuracy and precision of the scan to FEM process, further experimental results are required in order to fully validate this solution. However, this approach is highly promising given the high FEM to TSD accuracy compared to models from classic CAD to FEM approaches.

By removing CAD from the standard modeling workflow, the MORPH method was shown to vastly accelerate the mesh generation process and greatly increase the likelihood of model generation success. This automated mesh updating process requires only TSD obtained from a modern optical scanner and a single FEM either manually created from a sample of that scan data, or an as-designed FEM in order to determine the harmonic response of a mistuned population of IBRs or blades. This mesh updating approach could also be used for non-turbomachinery components for more accurate stress or modal analysis and has wide applicability across the field of engineering.

REFERENCES

[1] Srinivasan, A. V., 1997. "Flutter and resonant vibration characteristics of engine blades". *Journal of Engineering for Gas Turbines and Power,* ***119***(4), pp. 742–775.

[2] Griffin, J. H., and Hoosac, T. M., 1984. "Model development and statistical investigation of turbine blade mistuning". *Journal of Vibration, Acoustics, Stress, and Reliability in Design,* ***106***, pp. 204–210.

[3] Lee, S.-Y., Castanier, M. P., and Pierre, C., 2005. "Assessment of probabilistic methods for mistuned bladed disk vibration". In 46th AIAA/ASME/ASCE/AHS/ASC Structures, Structural Dynamics, and Materials Conference.

[4] Beck, J. A., Brown, J. M., Slater, J. C., and Cross, C. J., 2012. "Probabilistic mistuning assessment using nominal and geometry based mistuning methods". In Proceedings of the ASME Turbo Expo.

[5] Sinha, A., Hall, B., Cassenti, B., and Hilbert, G., 2008. "Vibratory parameters of blades from coordinate measurement machine data". *Journal of Turbomachinery,* ***130***(1).

[6] Beck, J., Brown, J., Slater, J., and Cross, C., 2013. "Probabilistic mistuning assessment using nominal and geometry based mistuning methods". *Journal of Turbomachinery,* ***135***(5).

[7] Hussain, M., Rao, S., and Prasad, K., 2008. "Reverse engineering: Point cloud generation with cmm for part modeling and error analysis". *ARPN Journal of Engineering and Applied Sciences,* ***3***(4), August, pp. 37–40.

[8] H. Huang, Z. Chen, X. Z., 2003. "Smart robitic system for 3d profile turbine vane airfoil repair". *International Journal of Advanced Manufacturing Technology,* ***21***, pp. 275–283.

[9] She, C., and Chang, C., 2007. "Study of applying reverse engineering to turbine blade manufacture". *Journal of Mechanical Science and Technology,* ***21***, pp. 1580–1584.

[10] Blacker, T., 1996. "The cooper tool". In 5th International Meshing Roundtable, SAND 95-2130, Sandia National Laboratories, pp. 13–29.

[11] Onate, E., 2012. Structural analysis with the finite element method. linear statics: Volume 1: Basis and solids (lecture notes on numerical methods in engineering and sciences).

[12] Benzley, S. E., Perry, E., Merkley, K., and Clark, B., 1995. "A comparison of all hexagonal and all tetrahedral finite element meshes for elastic and elasto-plastic analysis". In 4th International Meshing Round table Sandia National Labs.

[13] Entrekin, A., 1999. "Accuracy of msc/nastran first- and second-order tetrahedral elements in solid modeling for stress analysis". In MSC 1999 Aerospace Users' Conference Proceddings.

[14] Kaszynski, A., Beck, J., and Brown, J., 2013. "Uncertainties of an automated optical 3d geometry measurement, modeling, and analysis process for mistuned integrally bladed rotor reverse engineering". *Journal of Engineering for Gas Turbines and Power,* ***135***.

[15] Hoppe, H., DeRose, T., Duchamp, T., McDonald, J., and Stuetzle, W., 1992. "Surface reconstruction from unorganized points". In Proceedings of the 19th Annual Conference on Comptuer Graphics.

[16] Chang, K.-H., and Chen, C., 2011. "3d shape engineering and design parameterization". *Computer-Aided Design & Applications,* ***8***(5), pp. 681–692.

[17] Peyré, G., and Cohen, L., 2006. "Geodesic remeshing using front propagation". *International Journal of Computer Vision,* ***69***(1), pp. 145–156.

[18] Sheffer, A., Etzion, M., and Bercovier, M., 1999. "Hexahedral mesh generation using embedded voronoi graph". In In Proceedings of the 7th International Meshing Roundtable, pp. 347–364.

[19] Fabio, R., 2003. "From point cloud to surface: the modeling and visualization problem". *International Workshop on*

Visualization and Animation of Reality-based 3D Models, ***34***.

[20] Kanai, T., Suzuki, H., and Kimura, F., 1997. "3d geometric metamorphosis based on harmonic maps". In Proceedings of Pacific Graphics, pp. 97–104.

[21] Eck, M., DeRose, T., Duchamp, T., Hoppe, H., Lounsbery, M., and Stuetzle, W., 1995. "Multiresolution analysis of arbitrary meshes". In Proceedings of the 22nd annual conference on Computer graphics and interactive techniques, pp. 173–182.

[22] Sigal, I., Hardisty, M., and Whyne, C., 2007. Mesh-morphing algorthims for generation of specimen-specific finite element models of rat tail vertebrae.

[23] Besl, P., and McKay, N., 1992. "A method for registration of 3d shapes". *In IEEE Transactions on PAMI,* ***14***, pp. 239–256.

[24] Moller, T., and Trumbore, B., 1997. "Fast, minimum storage ray-triangle intersection". *Journal of Graphics Tools,* ***2***, pp. 21–28.

[25] Bottasso, C., Detomi, D., and Serra, R., 2005. "The ball-vertex method: A new simple spring analogy method for unstructured dynamic meshes". *Computer Methods in Applied Mechanics and Engineering,* ***194***, pp. 4244–4264.

[26] Brajlih, T., Tasic, T., Drstvensek, I., Valentan, B., and Hadzistevic, M., 2011. "Possiblities of using three-dimential optical scanning in complex geometrical inspection". *Journal of Mechanical Engineering,* ***57***, pp. 826–833.

[27] Jones, K., and Cross, C., 2003. "Traveling wave excitation system for bladed disks". *Journal of Propulsion and Power,* ***19***.